Unsteady Wave Structure near Separation in a Mach 5 Compression Ramp Interaction

Mehmet E. Erengil* and David S. Dolling†
University of Texas at Austin, Austin, Texas 78712

Fluctuating wall-pressure measurements have been made under the unsteady separation shock and the separated shear layer in a Mach 5 compression ramp-induced turbulent interaction. The freestream unit Reynolds number was 49.6×10^6 m^{-1} and the turbulent boundary layer developed on the tunnel floor under approximately adiabatic wall-temperature conditions. Conditional sampling and "variable-window" ensemble-averaging techniques have been used to determine ensemble-averaged pressure distributions for different separation shock-wave positions. The results show that 1) the region in which the separation shock foot translates is characterized by a compression system whose strength is a function of the separation shock position; 2) ensemble-averaged wall-pressure distributions for "shock-upstream" and "shock-downstream" conditions are characteristic of large- and small-scale separated flows, respectively, indicative of an expanding and contracting bubble; and 3) ensemble-averaged wall-pressure histories under the separated shear layer rise and fall as the separation shock translates downstream and upstream, respectively.

Introduction

IT has been known since the early 1950s that shock-induced turbulent boundary-layer separation, which is a feature of strong shock interactions, is unsteady.[1,2] Initial observations of the unsteadiness were made using optical methods that provided very little quantitative information other than approximate estimates of the shock motion length scale and its frequency. Kistler,[3] in 1964, was probably the first to make quantitative measurements in one such interaction induced by a forward-facing step, at Mach numbers of 3 and 4.5. Measurements of wall-pressure fluctuations near separation revealed the intermittent nature of the wall-pressure signal, which was attributed to the unsteady separation shock wave.

Several experimental studies in the late 1960s and early 1970s confirmed Kistler's findings and helped establish a database. The results of these studies and others are summarized in a recent review.[4] Much of this early work was motivated by the need to predict the fluctuating pressure field around high-speed vehicles, whereas the research of the past few years has focused more on the unsteadiness of the shock-induced separation process. Most of the recent work has been in unswept compression ramp flows at Mach numbers of 3 and 5,[5-9] and in interactions induced by blunt fins,[10] circular cylinders,[11-13] and sharp fins at angle of attack.[14-16] Some additional work, particularly relevant to the current study, has been done at Mach 2.85 in an interaction generated by a cylinder-flare model.[17]

This research has shown that a common feature of shock-induced turbulent separation is the low-frequency, large-scale motion of the separation shock. In this context, "low-frequency" means relative to the typical large eddy frequency in the incoming boundary layer. The term "large-scale" is used because the length of this "intermittent" region can be several boundary-layer thicknesses, δ_o, depending on the model geometry being tested.

For the two-dimensional compression ramp flows at supersonic speed, the generally accepted model of the flowfield is sketched in Fig. 1. This was determined by Settles[18] from pitot pressure, static pressure, and total temperature surveys. These measuring techniques have essentially zero frequency response, so this model represents a time-averaged picture. Since the separation shock wave is unsteady,[5] the question is raised as to whether Fig. 1 is an accurate representation of the flow structure, since it is the result of time-averaging different flowfields corresponding to different shock positions.

Kussoy et al.[17] have addressed this question, for the cylinder-flare interaction. In that study, simultaneous wall-pressure fluctuations, high-speed shadow movies, and LDV data were taken. Using a conditional sampling method, mean streamlines were calculated for "shock-forward" and "shock-back" positions and for the overall time-averaged cases. The shock-forward and shock-back cases were defined as when $P_s(t) \geq \bar{P}_s + \sigma_{P_s}$ and $P_s(t) \leq \bar{P}_s - 0.5\,\sigma_{P_s}$, respectively. Here, $P_s(t)$ is the instantaneous wall pressure, $\bar{P}_s$ the mean value, and σ_{P_s} the standard deviation, all measured at the mean shock position. The results showed that the separated bubble "expanded and contracted like a balloon." Gramann and Dolling have observed a similar phenomenon in flows induced by circular cylinders[19] and by unswept compression ramps.[9] In the latter studies, the instantaneous separation point was determined to be at, or just downstream of, the instantaneous shock foot, showing that the separation process itself is intermittent. The separation line determined by

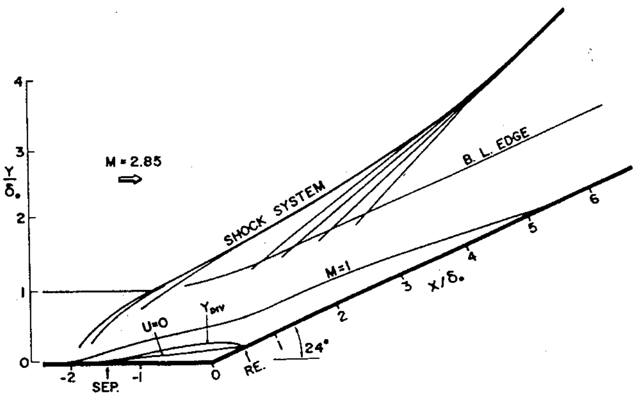

Fig. 1 Time-averaged flowfield (from Ref. 18).

Received July 10, 1989; revision received Feb. 26, 1990.

*Graduate Student, Department of Aerospace Engineering and Engineering Mechanics. Student Member AIAA.

†Associate Professor, Department of Aerospace Engineering and Engineering Mechanics. Associate Fellow AIAA.

surface-tracer techniques was at, or close to, the downstream boundary of the region of intermittent separation.

The focus of the current work was to examine some of these same questions in a Mach 5, 28 deg separated compression ramp flow. This paper focuses on the flowfield upstream of the corner; this includes the region of separation shock motion and intermittent separation, and the continuously separated flow upstream of the corner. The specific questions addressed are as follows:

1) As the separation shock translates streamwise is its strength constant, or is it a function of its position and/or its direction of motion?

2) What is the flow structure in the intermittent region? How does the strength of the compression waves just downstream of the separation shock vary with separation shock position and its direction of motion?

3) As the separation shock translates are there changes in the flow structure or are the changes simply in flowfield length scale? Do the ensemble-averaged pressures throughout the flowfield vary with separation shock position or are the unsteady effects local and confined largely to the intermittent region?

4) Is there any correlation between the separation shock motion and the ensemble-averaged pressure histories under the separated shear layer?

Experimental Program

Wind Tunnel and Model

The experiments were conducted in the Mach 5 blowdown tunnel of The University of Texas at Austin. This tunnel has a constant-area test section, which measures 17.78 × 15.24 cm (7 × 6 in.) in cross section and 30.48 cm (12 in.) in length. An 8.57 cm (3.375 in.) diameter brass plug, centered at 10.16 cm (4 in.) from the nozzle exit, was mounted flush with the tunnel floor as shown in Fig. 2. This plug has a row of 26 transducer ports along its centerline, spaced 0.292 cm (0.115 in.) center to center. During the tests, dummy brass plugs were mounted flush in any unused transducer ports.

The model used was a 28 deg unswept aluminum compression ramp, 12.70 cm (5 in.) wide and 3.81 cm (1.5 in.) high at the trailing edge. Aerodynamic fences with sharpened leading edges were attached to the ramp sides to avoid spanwise spillage and to isolate the interaction from the sidewall boundary layers. The leading edges of the fences extended 7.4 cm (2.9 in.) upstream of the compression corner on the tunnel floor. The model and the plug with transducer ports are sketched in Fig. 2.

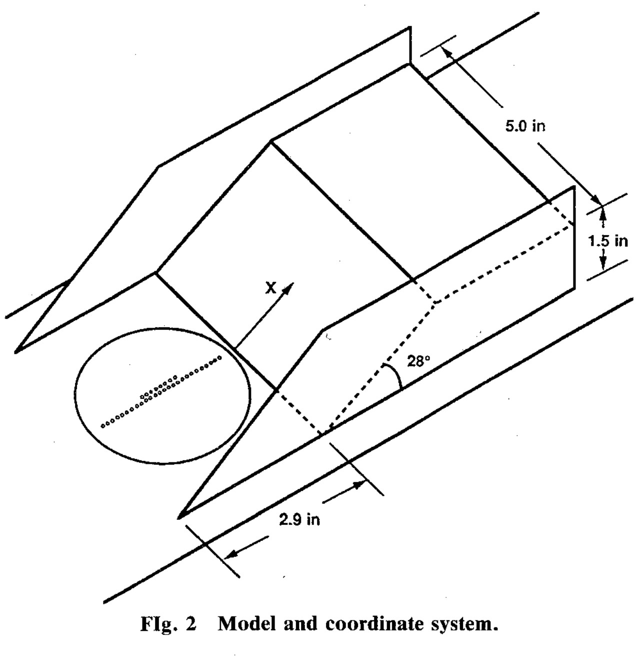

Fig. 2 Model and coordinate system.

Flow Conditions

The freestream total pressure and total temperature were 2.17×10^6 N/m^2 (315 psia) and 350 K (630°R), respectively. The freestream unit Reynolds number was 49.6×10^6 m^{-1} (15.1×10^6 ft^{-1}) and at the test station the freestream Mach number was 4.95. The incoming turbulent boundary layer underwent natural transition and developed under approximately adiabatic wall-temperature conditions. At the test station it was 1.75 cm (0.7 in.) thick. The boundary-layer and freestream flow properties were determined from pitot surveys made with a probe having a tip orifice 0.020 cm (0.008 in.) high and 0.038 cm (0.015 in.) wide. In the data reduction, the static pressure and total temperature were assumed constant through the boundary layer, with no heat transfer at the wall. Detailed information about the turbulent boundary-layer properties is given in Ref. 20.

Instrumentation

Up to eight Kulite pressure transducers were used to measure the wall-pressure fluctuations. These transducers have a nominal outer diameter of 0.159 cm (0.0625 in.) and a pressure-sensitive diaphragm 0.071 cm (0.028 in.) in diameter. Three of the transducers were model XCW-062-15A with a pressure range of 0–15 psia, and a diaphragm natural frequency of about 250 kHz. The other five transducers were model XCQ-062-50A with a pressure range of 0–50 psia, and a diaphragm natural frequency of about 500 kHz. Perforated screens protecting the diaphragms from dust particles limit the effective frequency response to about 50 kHz. The transducers were calibrated statically since it has been shown[21] that static calibrations differ from more accurate dynamic calibrations by only 2–3%. A Heise digital pressure gauge (Model 710A), accurate to within 7 N/m^2 (0.001 psia), was used for calibration.

Output from the pressure transducers was amplified by either Dynamics (Model 7525), Measurements Group (Model 2311) or PARC (Model 113) amplifiers, and then low-pass filtered using Ithaco (Model 4113 or Model 4213) analog filters, with the cut-off set at 50 kHz. Amplifier gain settings varied from 1500 to 9000, depending on the transducer type and its position in the interaction. Gain settings were adjusted before every calibration in order to maintain the maximum amplitude resolution, which was about 5 N/m^2 (0.0007 psia). The filtered signals were then digitized by the MASSCOMP 12-bit A/D converter equipped with sample-and-hold that outputs 0–4095 counts for inputs of 0–10 V. Noise on the data-acquisition system was typically ±7 A/D counts, resulting in signal-to-noise ratios that varied from about 10 (for measurements in the incoming boundary layer) to several 100 in most cases.

Data Acquisition

The measurements were made in two parts. In the first part, 100 records (1024 datapoints per record) per channel were simultaneously sampled from eight transducers at a rate of 110 kHz per channel. The spacing between two adjacent transducers ζ was 0.292 cm (0.115 in.), and the eight transducers were aligned streamwise spanning the intermittent region. In the second part, 200 records of data per channel were taken using only four transducers sampled at 200 kHz per channel. First, the general features of the interaction were obtained from several tests in which the four transducers, spaced 0.292 cm (0.115 in.) apart, were shifted progressively upstream from the compression ramp corner. Then, two transducers, also spaced 0.292 cm (0.115 in.) apart, were held fixed in the intermittent region and the other two (with a fixed separation distance) were moved downstream toward the ramp in increments of 0.58 cm (0.23 in.). The procedure was then repeated by moving the first two transducers to a new position in the intermittent region and moving the other two toward the corner, again in increments of 0.58 cm (0.23 in.). This was done to obtain simultaneous pressure measurements in the intermittent region and under the separated shear layer.

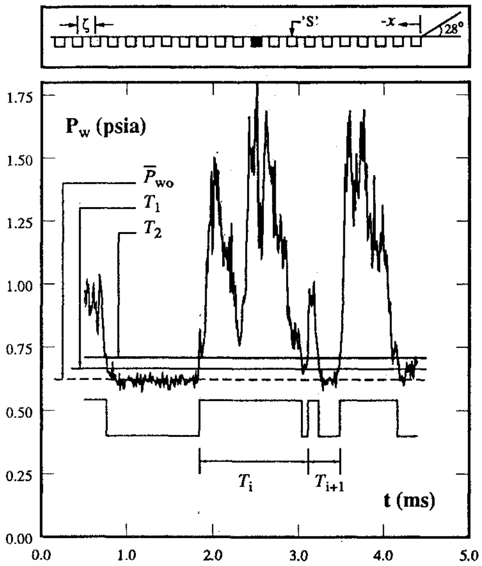

Fig. 3 Boxcar conversion technique.

Analysis Techniques

Standard time-series analysis techniques, and conditional sampling and ensemble-averaging techniques have been used to analyze the data. The latter techniques are discussed below.

Conditional Sampling

Wall-pressure signals in this type of flow have frequencies and amplitudes representative of different flow phenomena, such as the relatively low-frequency, large-amplitude fluctuations generated by the unsteady separation shock superimposed on the high-frequency, low-amplitude fluctuations of the undisturbed boundary layer, and the high-frequency, large-amplitude fluctuations generated by the separated turbulent shear layer superimposed on the lower-frequency global motion of the separation "bubble." Conditional sampling algorithms have been used to isolate the different phenomena, study them separately, and then piece the results back together into a coherent physical picture.

One such algorithm, which separates the relatively low-frequency, large-scale separation shock motion from both the high-frequency, low-amplitude pressure fluctuations in the incoming boundary layer, and the high-frequency, higher-amplitude pressure fluctuations of the separated shear layer downstream of the separation shock, is based on a two-threshold method (2TM) boxcar conversion technique. This conversion, which is shown in Fig. 3, permits calculation of the shock zero-crossing frequency f_c and other statistics of the shock motion. The zero-crossing frequency is given by

$$f_c = 1 \Bigg/ \left(\frac{1}{N} \sum_{i=1}^{N} T_i \right)$$

where T_i is the ith shock period, as defined in Fig. 3, and N is the number of shocks. This method is explained in detail in Ref. 12. In brief, the two thresholds are set at $T_1 = \bar{P}_{wo} + 3\sigma_{P_{wo}}$ and $T_2 = \bar{P}_{wo} + 6\sigma_{P_{wo}}$, where $\bar{P}_{wo}$ is the mean pressure of the undisturbed turbulent boundary layer and $\sigma_{P_{wo}}$ the rms value of the turbulent boundary-layer fluctuations. These threshold settings were recommended following a sensitivity analysis of the effects of T_1 and T_2.[12] It should be noted that these settings provided an optimum discrimination between the relatively low-frequency, large-amplitude pressure fluctuations due to shock motion and the high-frequency turbulent fluctuations in the downstream boundary layer (see also Ref. 12). The boxcar is generated when $P_w(t) > T_2$ and is terminated when $P_w(t) < T_1$. Thus, when the boxcar assumes a value of 1, this signifies a shock passage in the upstream direction and is called the rise time (or "rise"). Similarly, when the boxcar assumes a value of 0, this signifies a downstream shock passage and is called the fall time (or "fall"). Hence, each shock passage is characterized by a rise time and a corresponding fall time. These times are the only pertinent information in the analysis of the separation shock motion.

In the current study, a third threshold T_3 was introduced in addition to T_1 and T_2. This third threshold is needed to determine the shock fall times more accurately. In prior analyses, most of the separation shock statistics were calculated using only the rise times, which are more easily determined than the fall times. In the current study, however, an accurate measurement of the fall times is imperative, because they directly influence separation shock statistics. Since the rise time is used to determine when the shock is at a specific position (this is discussed in more detail in the next section), T_3 was set equal to T_2 so that the fall time would correspond to exactly the same shock position. In this case, T_3 was used to monitor the fall times as follows. Once a shock passage was detected using T_1 and T_2, and an initial fall time was assigned, a counter was then used to march backward in time until the instantaneous value $P_w(t)$ was found that was just below T_3. The fall time was then reassigned to this new value. The significance of this improvement will be clearer later, when the statistics of the upstream and downstream shock passages are compared.

Variable-Window Ensemble-Averaging

Ensemble-averaging was performed on all channels and was triggered by a shock passage, either in the upstream direction (rise) or downstream direction (fall) over the transducer(s) in the intermittent region. The purpose was to determine if there was a correlation between the separation shock position and the ensemble-averaged pressure level under the separated shear layer, and between the separation shock motion and ensemble-averaged pressure history under the separated shear layer. Since the separation shock has a wide range of periods, a "variable-window" ensemble-averaging technique was used to ensure that data corresponding to upstream shock passages were separated from those for downstream passages. The width of the window W for any particular shock passage was set by considering both the preceding and following shock passages. For example, in the case of an upstream passage, a rise is preceded by a fall and followed by another fall, as shown by the two examples in Fig. 4a. The variable-window extends from the middle of the fall-rise pair to the middle of the rise-fall pair and is "centered" at the rise time, which is assigned the value of $\tau = 0$, as indicated. Therefore, for a fixed transducer the $\tau = 0$ value corresponds essentially to the "freezing" of the separation shock at a given position as it sweeps upstream (i.e., that of the transducer indicated in the schematic at the top of Fig. 4a). Hence, $\tau < 0$ corresponds to times when the shock is downstream of that position, and $\tau > 0$ corresponds to times when it is upstream of that position. It should be noted that τ is not normalized by the window width W.

Once the center and width of the window are determined from a given shock passage, the data spanning the window are extracted from all channels to form one ensemble for each channel. The procedure is then repeated for all subsequent shock passages, and the corresponding ensembles are averaged to form ensemble-averaged pressure histories at each station. For example, Figs. 4a and 4b show simultaneously sampled signals on the triggering channel and on the measuring channel downstream of separation, respectively. The two ensembles corresponding to the two windows shown in parts (a) and (b) are extracted from the original signals, and are shown for the triggering channel in Fig. 4c, and for the measuring channel in Fig. 4d, in the relative time domain τ. Finally, the pressure histories of the two channels, ensemble-averaged over many windows (of order several hundred), are shown in parts (e) and (f) of Fig. 4, respectively. It should be noted that, for any value of τ, the number of ensembles that the final result is

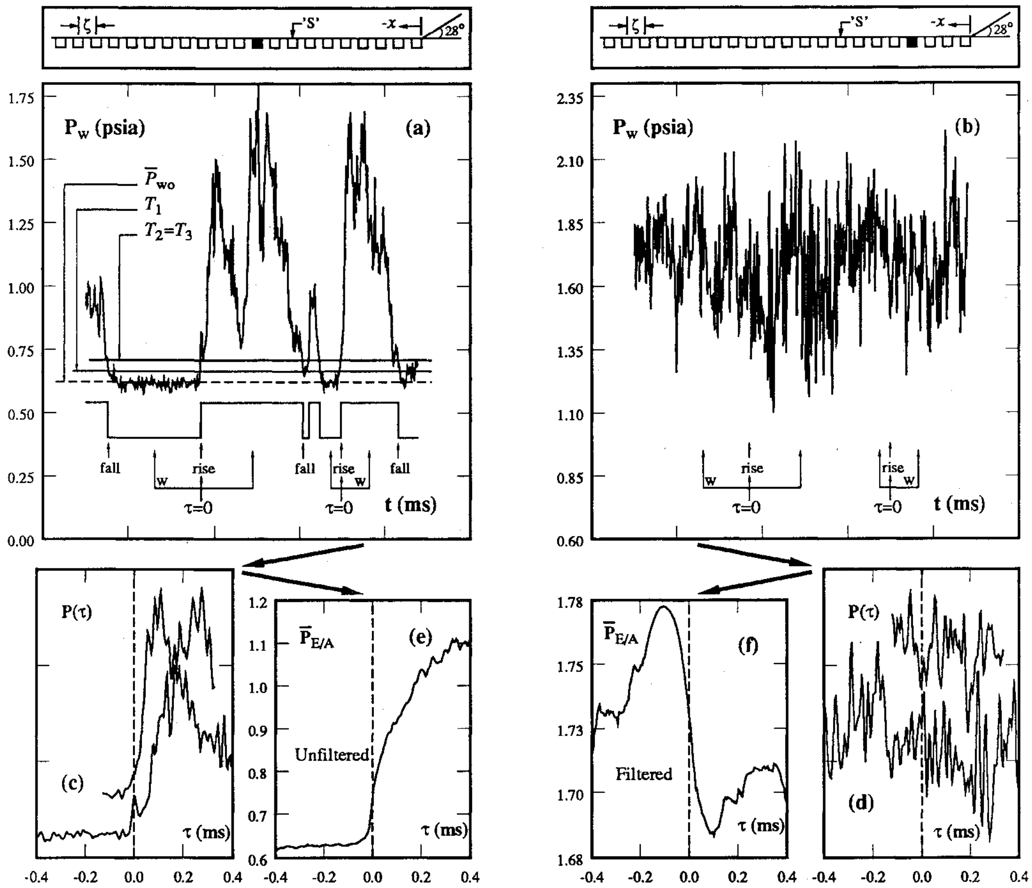

Fig. 4 Variable-window ensemble averaging.

based on will vary, since W changes from one ensemble to another.

Discussion of Results

Basic Features of the Interaction

Distributions of the normalized mean wall pressure $\bar{P}_w/\bar{P}_{wo}$ and the standard deviation σ_{P_w} vs the nondimensional streamwise distance x/δ_o from the corner are shown in Fig. 5. Subscript "o" refers to undisturbed conditions just upstream of the interaction. For clarity, σ_{P_w} has been multiplied by 10 and then shifted upward two units. Also, σ_{P_w} has not been normalized by $\sigma_{P_{wo}}$ since the latter value is almost certainly underestimated due to the frequency-response limitations of the transducer. The theoretical inviscid pressure ratio is indicated by the solid line. The scatter in the mean pressure distribution is indicative of the difficulties of measuring low pressures (i.e., a few psia) using high-frequency response transducers with ranges up to 50 psia. The consistency in the rms measurements, on the other hand, show the good repeatability of the experiments from run to run. Detailed spanwise measurements in the same flowfield have shown that the intermittent region is two-dimensional in a time-averaged sense.[22] Also shown in the figure are the locations of the separation line S and the reattachment line R as deduced from surface flow patterns obtained using a mixture of diesel fuel and blue chalk powder.[22] The upstream influence line UI is also indicated.

The intermittency γ at a given station is defined as the percentage of time that the separation shock is upstream of that station. Discrete values of γ, as well as those of the zero-crossing frequency f_c, are plotted vs x/δ_o in Fig. 6. The solid lines pass through the average values at each station. The dashed line is the error function fit to the intermittency data. The good fit shows that separation shock crossings are essentially randomly distributed within the intermittent region. Thus, the probability of finding a shock passage is at a maximum near $\gamma = 0.5$, and it decreases to zero upstream of UI and downstream of S. This result is also seen in the zero-crossing frequency distribution that has a maximum value of about 1.0 kHz at $\gamma \approx 0.5$. In this flow, the length of the intermittent region is about 1.6 δ_o. It should be noted that the streamwise distance has been expressed in terms of δ_o for convenience, not because δ_o is the appropriate scaling parameter.

Power spectra at five different positions in the interaction are shown in Fig. 7. The normalized form, $G(f)\cdot f/\sigma^2_{P_w}$, has been used except for the incoming turbulent boundary layer that is shown in dimensional form, $G(f)\cdot f$, due to the difficulties of accurately measuring $\sigma_{P_{wo}}$. The incoming boundary layer (curve 1) has a broadband spectrum; however, the con-

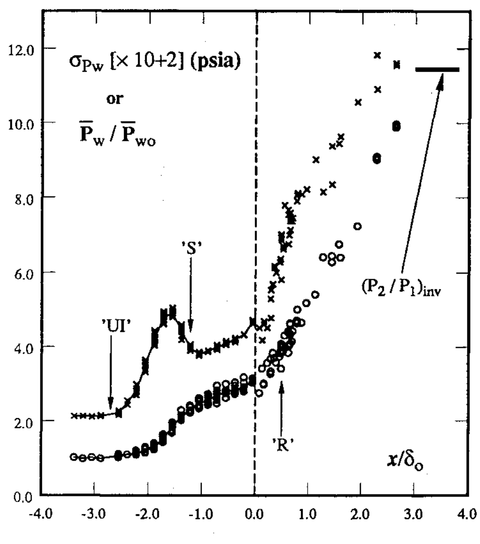

Fig. 5 Standard deviation and normalized mean pressure distributions.

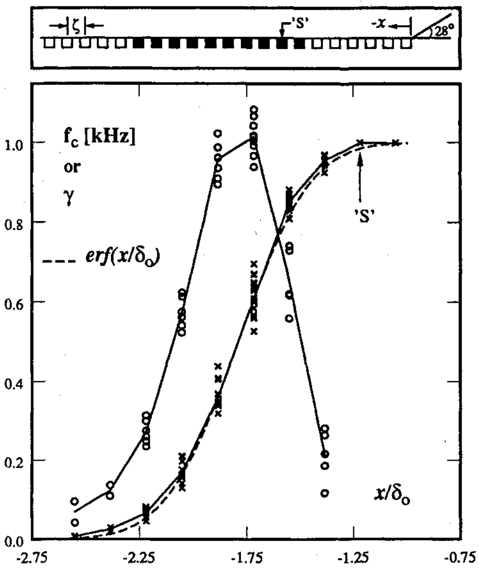

Fig. 6 Intermittency and zero-crossing frequency distributions.

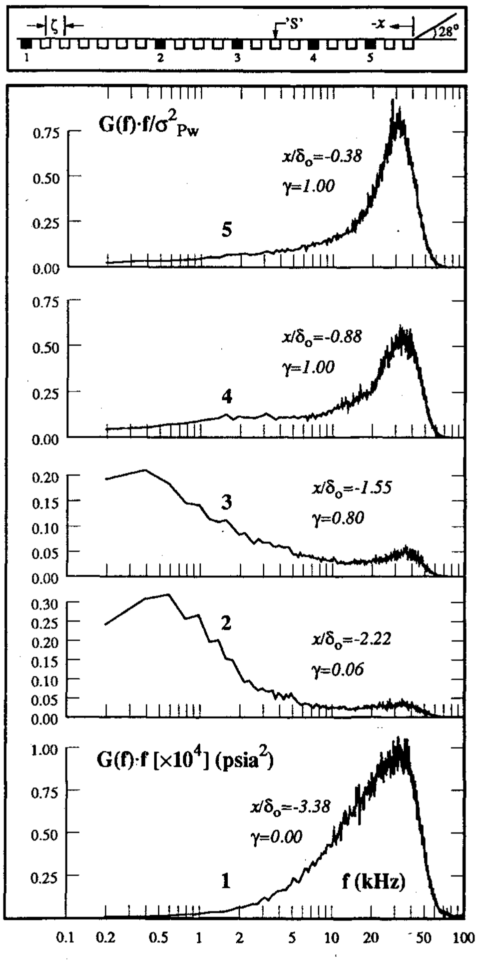

Fig. 7 Streamwise evolution of power spectral densities.

tribution to the variance from the low frequencies is quite small, and as expected, most of the energy is in the high-frequency fluctuations. In the intermittent region (curves 2 and 3), the wall-pressure signal is dominated by the relatively low-frequency, high-amplitude pressure fluctuations due to the shock motion. More than 90% of the variance is from frequencies less than 20 kHz. The center frequency, which indicates the characteristic frequency of the higher-amplitude pressure fluctuations due to shock passages, occurs at about 400–500 Hz, regardless of the position in the intermittent region. This dominance by the relatively low-frequency, high-amplitude pressure fluctuations is preserved even at the downstream end of the intermittent region, where the high-frequency, high-amplitude pressure fluctuations of the turbulent shear layer are a larger fraction of the signal and begin to contribute more to the variance. Even though the high-frequency content of the shear-layer fluctuations becomes more and more dominant (curves 4 and 5), the low-frequency unsteadiness persists as far downstream as the compression ramp corner.

In the incompressible turbulent separated flow experiments of Kiya and Sasaki,[23,24] the characteristic Strouhal number, St ($\equiv fL_s/U_\infty$), of the separation bubble unsteadiness was 0.12, where L_s is the bubble length, U_∞ the freestream velocity, and f the center frequency of the spectrum of the wall-pressure signal. In the current experiment, the Strouhal number, formed the same way, is about 0.03. If the maximum zero-crossing frequency is used instead of the center frequency, then the value is about 0.06. In Refs. 23 and 24, the Strouhal number of the low-frequency unsteadiness was less than about 0.2 with a peak of 0.12 as stated above. In the current experiment, in which the shock and bubble frequencies are less than 3–4 kHz, the corresponding Strouhal numbers are about 0.18–0.24. However, it should be noted that at this stage there is little evidence to suggest that in the high-speed case, U_∞ and L_s are appropriate normalizers. More work under different flow conditions is needed to evaluate this.

Separation Shock Wave Strength as a Function of Position

Figure 8 shows ensemble-averaged pressure histories at three stations in the intermittent region for the case of an upstream motion of the separation shock. The intermittency values at these stations are indicated in the insert. The schematic at the top of the figure shows the transducer stations upstream of the ramp corner. Filled markers indicate the positions for which ensemble-averaged pressure histories are shown in the figure, and the crossed ones indicate positions of the other simultaneously sampled channels. Also shown in the sketch is the separation shock, the foot of which, for this case, is at station n. The counter i indicates the distance from the shock foot to the position of interest and is given in terms of the number of transducer spacings, ζ. At $\tau = 0$, the shock has just crossed channel n, moving in the upstream direction. For $\tau < 0$, the shock is downstream of channel n, and for $\tau > 0$, it is

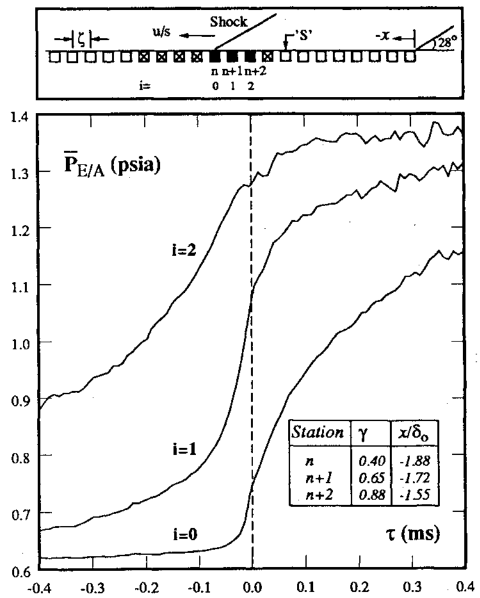

Fig. 8 Ensemble-averaged pressure histories in the intermittent region.

upstream of channels n, $n+1$, and $n+2$. Since $\tau = 0$ corresponds essentially to the "freezing" of the shock at channel n, the ensemble-averaged pressure value at $\tau = 0$ at station $n+1$ can be used to define the separation shock strength at position n. Hence, separation shock strength at station n, $(\Delta Ps)_1^n$, is defined as the difference between the ensemble-averaged pressure at $\tau = 0$ on channel $n+1$ and the pressure of the undisturbed boundary-layer component of the signal as measured by the same channel, $n+1$. Defining the shock strength in this way avoids any ambiguities with respect to whether the shock has actually crossed the transducer and eliminates any transducer zero-shift and temperature drift problems that may occur. This process can also be carried out for the shock moving in the downstream direction. It should be noted that, with this definition, $(\Delta Ps)_1^n$ includes not only the pressure rise due to the separation shock, but also the small increase in pressure due to any compression between the separation shock and the next transducer downstream.

In Fig. 9, shock strength $(\Delta Ps)_1^n$ for both upstream and downstream motions of the separation shock is plotted vs the normalized distance x/δ_o from the corner. The importance of the third threshold T_3 should now be clear, because if it were not introduced, the shock position at fall times would have been slightly different than that at rise times. However, this is not the case using T_3, and the separation shock strength for upstream motion can be compared directly with that of downstream motion. Also shown in Fig. 9 are the average intermittency values at each station. At low γ, the separation shock strength increases rather gradually, but is followed by a more rapid increase at higher intermittencies. Overall, the separation shock strength increases by about 50% as the shock moves from the lowest γ to the highest. This result is independent of the direction of motion of the shock.

Ensemble-Averaged Compression Structure in Intermittent Region

It had been concluded in earlier work, Ref. 7, that the mean pressure distribution in the intermittent region is generated by a single shock of constant strength undergoing random motion. Current results from the ensemble-averaging technique show very clearly that not only does the separation shock vary in strength as it translates, but so do the compression waves following the separation shock.

In Fig. 8, it can be seen that the pressure rise above the undisturbed boundary-layer value at station $n+2$, $(\Delta P)_2^n$, is due to the shock at n [i.e., $(\Delta Ps)_1^n$], and compression waves between stations $n+1$ and $n+2$. The contribution from the com-

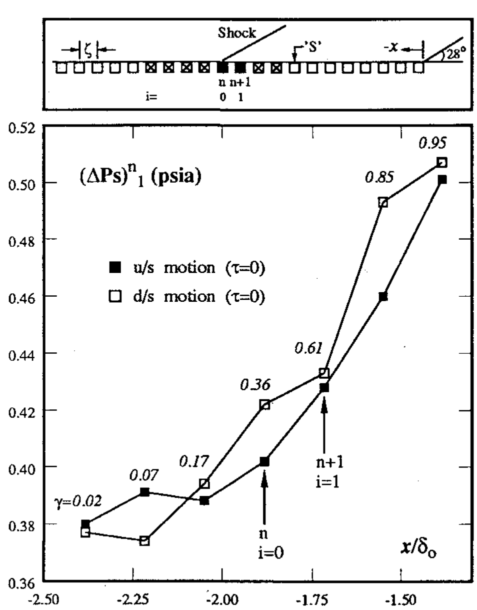

Fig. 9 Separation shock wave strength variation with position.

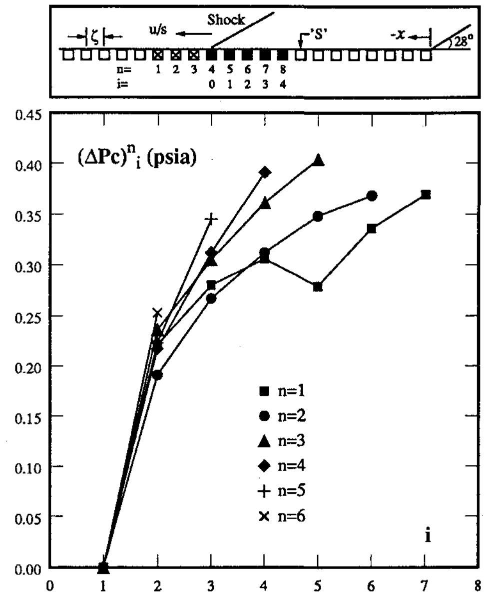

Fig. 10 Ensemble-averaged compression wave structure.

pression waves will be defined as $(\Delta Pc)_2^n$. Clearly, $(\Delta Pc)_2^n$ is simply the difference between $(\Delta P)_2^n$ and $(\Delta Ps)_1^n$. Similarly, at station $n+3$ the pressure rise is due to $(\Delta Ps)_1^n$ and the compression waves between stations $n+1$ to $n+3$ that, if we use the preceding terminology, is given by $(\Delta Pc)_3^n$. In general, $(\Delta Pc)_i^n$ can be obtained for $1 \leq n \leq N$ and $0 \leq i \leq (N-n)$, where N is the total number of simultaneously sampled channels of data, n the shock position indicator (i.e., the triggering channel), and i the number of transducer spacings from the shock foot. In an example case, shown in the schematic at the top of Fig. 10, with eight streamwise transducers, the shock foot is sketched at $n = 4$. For this case, $N = 8$, therefore, $1 \leq i \leq 4$.

In Fig. 10, $(\Delta Pc)_i^n$ is plotted for $1 \leq i \leq (N-n)$ with the shock position n as the parameter. It is clear that, for a fixed n, the pressure downstream of the shock foot increases with distance from the shock, but at a decreasing rate. At any fixed position in the intermittent region, the separation shock is followed by compression waves that decrease in strength with distance from the shock. The increase in the slopes of these curves with increasing n further shows that the compression waves following the shock become stronger as the shock moves downstream (i.e., as n increases). It should be noted that this figure is only for those ensemble-averaged pressures for the separation shock moving upstream. Similar results were obtained for the downstream motion of the separation shock.

Ensemble-Averaged Wall Pressures

Ensemble-averaged pressures $\bar{P}_{E/A}$ from the shock foot to the ramp corner, generated by freezing the shock at various positions in the intermittent region, are plotted vs x/δ_o in Fig. 11. In the schematic at the top of the figure, filled markers show an example of four simultaneously sampled transducer positions. (The "crossed" markers indicate the other positions at which ensemble-averaged pressures were obtained.) Again, n represents the position of the shock in the intermittent region, and i is used to indicate the distance from the foot of the separation shock to the position of interest. Also shown by a solid line in the same figure is the mean pressure distribution, obtained by averaging at each station the mean pressure values that were presented earlier (Fig. 5). Each one of the dashed-line curves was generated by freezing the shock at a given position in the intermittent region as it moved upstream. Two features are evident. First, $\bar{P}_{E/A}$ in the separated flow within about 1 δ_o upstream of the ramp corner is relatively insensitive to the shock position in the intermittent region (i.e., the difference between the shock-upstream and shock-downstream values is only a few percent). Second, for the shock-upstream case, the ensemble-averaged pressure distribution has a well-defined plateau region, consistent with a large-scale separated flow. As the shock moves toward its most downstream position, the ensemble-averaged pressure distribution progressively changes, finally resembling that typical of a small-scale separated flow. This picture is entirely consistent with the work of Gramann and Dolling,[19] in which it is shown that the instantaneous separation point essentially follows the shock foot. Again, the data presented are for upstream motion of the separation shock, but similar results were obtained for downstream motion as well.

Ensemble-Averaged Pressure Histories

Up to this point, the discussion of the ensemble-averaged results has focused on the shock position only (i.e., the "frozen" flowfield, or $\tau = 0$ values). It should be noted that this does not properly address the question of any correlation between the separation shock motion and dynamics of the separation bubble. The reason for this is the following. The unsteadiness of the separation shock is characterized by random motions with a range of speeds and length scales. The length scale as defined here means the distance the shock moves before it changes its direction of motion. Just knowing the position of the shock and its direction of motion does not provide specific information about the unsteady behavior at stations further downstream. In other words, $\tau = 0$ values measured at different stations downstream for different fixed shock positions cannot be used to discuss the dynamics of the interaction, because these values do not have any history associated with them. For example, in Fig. 11, it is obvious that there must be large-scale motion of the separation shock, but the dynamics of the flowfield cannot be deduced from this figure, because it cannot be inferred that the ensemble-averaged pressure distributions occur sequentially (i.e., they have no history).

To address the question of a correlation between the separation shock motion and the pressures under the separated shear layer, rather than the separation shock position and the pressures under the separated shear layer, the ensemble-averaged pressure histories under the separated bubble must be examined, rather than the one particular value (i.e., $\tau = 0$) corresponding to a single separation shock position. Typical ensemble-averaged pressure histories in the intermittent region are shown in Fig. 12 for upstream and downstream motions of the separation shock, respectively. The relative position of the transducer is indicated in the schematic at the top of the figure. The pressure histories in Fig. 12 were calculated from the unfiltered signals. The corresponding simultaneous pressure histories measured under the separated shear layer are shown in Fig. 13 for upstream and downstream motions of the separation shock, respectively. The signal under the shear layer was first low-pass filtered at 10 kHz and then ensemble-averaged. It should be noted that the same trends are evident with or without filtering the original signal; however, the results become more pronounced when the signal is low-pass filtered. Further, since the wall-pressure signal under the separated shear layer is dominated by high-frequency, high-amplitude pressure fluctuations generated by turbulence, it was sometimes necessary to filter out these fluctuations, particularly in those cases calculated from a small number of ensembles. The filter cut-off frequency was set at 10 kHz, because the shock frequency distributions, calculated earlier, from the boxcar signals showed that the maximum shock frequencies were always substantially less than this value.

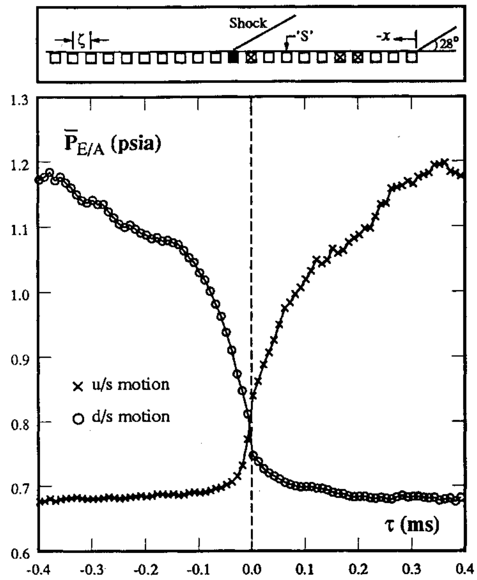

Fig. 12 Ensemble-averaged pressure histories in the intermittent region for upstream and downstream shock motions (simultaneous data in Fig. 13).

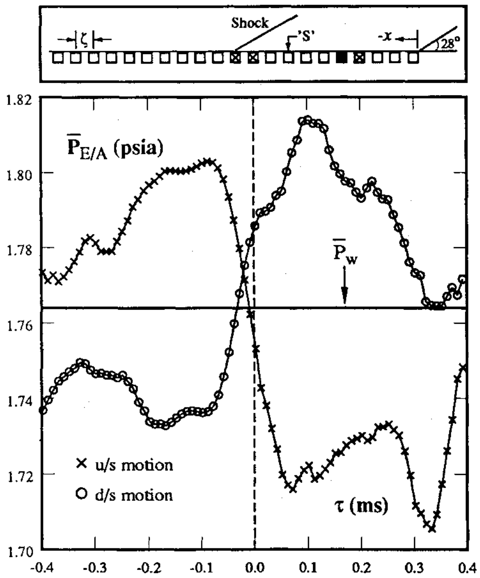

Fig. 13 Ensemble-averaged pressure histories under the separated shear layer for upstream and downstream shock motions (simultaneous data in Fig. 12).

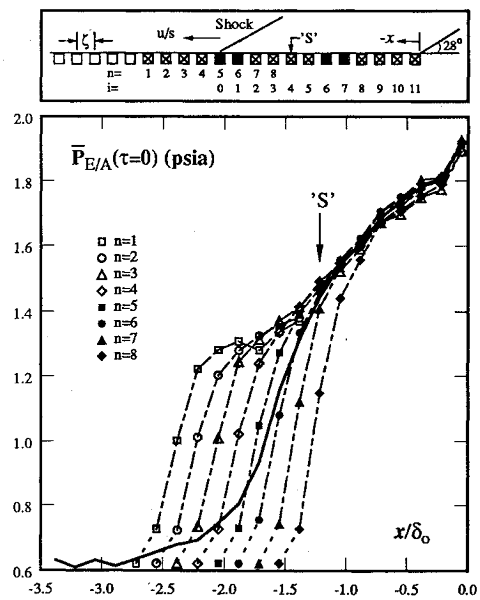

Fig. 11 Ensemble-averaged pressure distributions.

Clearly, as the separation shock wave moves upstream and weakens, the ensemble-averaged pressure under the separated shear layer drops. Conversely, as the shock moves downstream and strengthens, the ensemble-averaged pressure under the separated shear layer rises. This shows distinctly the correlation between the separation shock motion and the ensemble-averaged pressure histories under the separated shear layer. As mentioned earlier, the separation shock undergoes motions with a range of velocities and length scales, and each type of motion influences the ensemble-averaged pressure histories differently. For example, in the case of faster-moving shocks, the gradient of the ensemble-averaged pressure histories around $\tau = 0$ is steeper. Examples of these specific correlations are not presented here, but rather the overall picture is presented. Even so, the ensemble-averaged pressure histories of Figs. 12 and 13, which include data for a wide range of shock speeds and length scales, show very clearly that the separated bubble pressure levels fall and rise as the separation shock moves upstream and downstream, respectively.

Conclusions

Fluctuating wall-pressure measurements have been made upstream of the corner in a separated Mach 5 compression ramp interaction. The objective was to examine the unsteady compression wave structure near separation and its influence on the pressure levels and histories under the separated shear layer. The results can be summarized as follows.

1) The separation shock wave strength is a function of position in the intermittent region and increases with increasing intermittency. This result is independent of the direction of motion of the separation shock wave.

2) The flow structure in the intermittent region is not that of a single shock front undergoing random motion, as speculated in earlier work. In this region, the separation shock wave is followed by compression waves whose strength decreases with distance from the shock foot. Further, the compression following the separation shock becomes stronger as the shock moves downstream. This structure is also independent of the direction of motion of the separation shock.

3) Ensemble-averaged pressure distributions show how the mean flowfield is generated through the time-averaging of the different flowfields corresponding to different shock positions. Ensemble-averaged pressure distributions for shock-upstream and shock-downstream cases resemble typical mean pressure distributions for large- and small-scale separated flows, respectively.

4) Finally, there is a correlation between the separation shock motion and the ensemble-averaged pressure histories under the separated shear layer. The separation bubble pressures rise and fall as the separation shock moves downstream and upstream, respectively, showing that the separation shock motion correlates with the low-frequency pressure fluctuations of the separated bubble.

Acknowledgments

Support from AFOSR under Grant 86-0112, monitored by L. Sakell, is gratefully acknowledged.

References

[1]Bogdonoff, S. M., "Some Experimental Studies of the Separation of Supersonic Turbulent Boundary Layers," Rept. 336, Aero. Eng. Dept., Princeton Univ., Princeton, NJ, June 1955.

[2]Chapman, D. R., Kuehn, D. M., and Larson, H. K., "Investigation of Separated Flows in Supersonic and Subsonic Streams with Emphasis on the Effect of Transition," NACA TN 3869, March 1957.

[3]Kistler, A. L., "Fluctuating Wall Pressure Under Separated Supersonic Flow," *Journal of Acoustical Society of America,* Vol. 36, March 1964, pp. 543–550.

[4]Dolling, D. S., and Dussauge, J. P., "Fluctuating Wall Pressure Measurements," "A Survey of Measurements and Measuring Techniques in Rapidly Distorted Compressible Turbulent Boundary Layers," AGARDograph 315, Nov. 1988, Chap. 8.

[5]Dolling, D. S., and Murphy, M. T., "Unsteadiness of the Separation Shock Wave Structure in a Supersonic Compression Ramp Flowfield," *AIAA Journal,* Vol. 21, No. 12, 1983, pp. 1628–1634.

[6]Dolling, D. S., and Or, C. T., "Unsteadiness of the Shock Wave Structure in Attached and Separated Compression Ramp Flowfields," *Experiments in Fluids,* Vol. 3, 1985, pp. 24–32.

[7]Muck, K. C., Andreopoulos, J., and Dussauge, J. P., "Unsteady Nature of Shock-Wave/Turbulent Boundary-Layer Interactions," *AIAA Journal,* Vol. 26, No. 2, 1988, pp. 179–187.

[8]Andreopoulos, J., and Muck, K. C., "Some New Aspects of the Shock Wave Boundary Layer Interaction in Compression Ramp Flows," AIAA Paper 86-0342, Jan. 1986.

[9]Gramann, R. A., and Dolling, D. S., "Dynamics of Separation and Reattachment in a Mach 5 Unswept Compression Ramp Flow," AIAA Paper 90-0380, Jan. 1990.

[10]Dolling, D. S., and Bogdonoff, S. M., "An Experimental Investigation of the Unsteady Behavior of Blunt Fin-Induced Shock Wave Turbulent Boundary Layer Interactions," AIAA Paper 81-1287, AIAA 14th Fluid Dynamics, Plasma Dynamics and Lasers Conference, Palo Alto, CA, June 1981.

[11]Dolling, D. S., and Smith, D. R., "Separation Shock Dynamics in Mach 5 Turbulent Interactions Induced by Cylinders," *AIAA Journal,* Vol. 27, No. 12, 1989, pp. 1698–1706.

[12]Dolling, D. S., and Brusniak, L., "Separation Shock Motion in Fin, Cylinder, and Compression Ramp-Induced Turbulent Interactions," *AIAA Journal,* Vol. 27, No. 6, 1989, pp. 734–742.

[13]Dolling, D. S., and Narlo, J. C., II, "Driving Mechanism of Unsteady Separation Shock Motion in Hypersonic Interactive Flow, Aerodynamics of Hypersonic Lifting Vehicles," AGARD-CP-428, Nov. 1987.

[14]Tran, T. T., Tan, D. K. M., and Bogdonoff, S. M., "Surface Pressure Fluctuations in a Three-Dimensional Shock/Wave Turbulent Boundary Layer Interaction at Various Shock Strengths," AIAA Paper 85-1562, July 1985.

[15]Tan, D. K. M., Tran, T. T., and Bogdonoff, S. M., "Surface Pressure Fluctuations in a Three-Dimensional Shock Wave Turbulent Boundary Layer Interaction," AIAA Paper 85-0125, Jan. 1985.

[16]Tran, T. T., "An Experimental Investigation of Unsteadiness in Swept Shock Wave/Turbulent Boundary Layer Interactions," Ph.D. dissertation, Mechanical and Aerospace Engineering Dept., Princeton Univ., Princeton, NJ, Oct. 1986.

[17]Kussoy, M. I., Brown, J. D., Brown, J. L., Lockman, W. K., and Horstman, C. C., "Fluctuations and Massive Separation in Three-Dimensional Shock-Wave/Boundary-Layer Interactions," 2nd International Symposium on Transport Phenomena in "Turbulent Flows," Univ. of Tokyo, Oct. 25–29, 1987.

[18]Settles, G. S., Vas, I. E., and Bogdonoff, S. M., "Details of a Shock Separated Turbulent Boundary Layer at a Compression Corner," *AIAA Journal,* Vol. 14, No. 12, 1976, pp. 1709–1715.

[19]Gramann, R. A., and Dolling, D. S., "Detection of Turbulent Boundary Layer Separation Using Fluctuating Wall Pressure Signals," AIAA Paper 88-4676, Sept. 1988.

[20]Nordyke, R. J., "Spanwise Properties of the Unsteady Separation Shock in a Mach 5 Unswept Compression Ramp Interaction," M.S. thesis, Dept. of Aerospace Engineering and Engineering Mechanics, Univ. of Texas, Austin, TX, Dec. 1987.

[21]Raman, K. R., "A Study of Surface Pressure Fluctuations in Hypersonic Turbulent Boundary Layers," NASA CR-2386, Feb. 1974.

[22]Marshall, T. A., and Dolling, D. S., "Spanwise Properties of the Unsteady Separation Shock in a Mach 5 Unswept Compression Ramp Interaction," AIAA Paper 90-0377, Jan. 1990.

[23]Kiya, M., and Sasaki, K., "Structure of a Turbulent Separation Bubble," *Journal of Fluid Mechanics,* Vol. 137, Dec. 1983, pp. 83–113.

[24]Kiya, M., and Sasaki, K., "Structure of Large-Scale Vortices and Unsteady Reverse Flow in the Reattaching Zone of a Turbulent Separation Bubble," *Journal of Fluid Mechanics,* Vol. 154, May 1985, pp. 463–491.